COBEM 2021 26th International Congress of Mechanical Engineering
ABCM Associação Brasileira de Engenharia e Ciências Mecânicas
November 22-26, 2021, Virtual Congress, Brazil

COB-2021-0195
NUMERICAL ANALYSIS OF THE THERMODYNAMIC PERFORMANCE OF AN ACTIVE BAROCALORIC REGENERATOR USING PDMS RUBBER FOR REFRIGERATION APPLICATIONS

Pedro Henrique Oliveira Faria[1,*]
Kimi Shibuya Portugual[1]
Alexandre Magnus Gomes Carvalho[2,3]
Paulo Vinicius Trevizoli[1]

[1]Department of Mechanical Engineering, Federal University of Minas Gerais (UFMG), Belo Horizonte 31270-901, MG, Brazil
[2]Departamento de Engenharia Química, Universidade Federal de São Paulo, Diadema 09913-030 SP, Brasil
[3]Instituto de Física Armando Dias Tavares, Universidade do Estado do Rio de Janeiro, Rio de Janeiro 20550-013, RJ, Brasil.
*Corresponding author: pedrohofaria@gmail.com

Abstract. *Solid-state caloric cooling systems have been under research for some decades but in general, still have not reached the same performance metrics as vapor compression cooling devices. At the same time, environmental concerns related to refrigerant fluids have been growing. In addition, giant barocaloric effects have been recently discovered in elastomers, but there is still a lack of theoretical models reported in the literature to evaluate their potential to be applied as solid-state refrigerants in active caloric regenerators. This research contributes to fill this gap by proposing a mathematical model with a hybrid analytical-numerical solution for the fluid flow and heat transfer problems in an idealized barocaloric refrigerator using PDMS rubber as the refrigerant. Simulations are performed to investigate the influence of some geometric and operational parameters on the cooling capacity. It was found a maximum of 21.4 K temperature span under no-load conditions, and a maximum cooling capacity of 59.4 W at zero temperature span.*

Keywords: *active caloric regenerator, barocaloric effect, elastomers, refrigeration, Finite Volume Method*

1. INTRODUCTION

Though vapor compression technology for heating and cooling applications is widespread in society, restrictions imposed upon the working fluids are escalating, whether they are relative to environmental impact, user safety, or energetic performance of the equipment (Calm, 2008; Coulomb, 2006). The International Institute of Refrigeration (IIR) estimates that about 5 million refrigerators, air-conditioners, and heat pumps are used around the world, being responsible for the consumption of 20% of all the energy produced (IIR, 2019). This context motivates research on alternative technologies, notably i-caloric effects in solid-state refrigerants.

Among the i-caloric effects, stand out the barocaloric effect (BCE) which, despite being the less explored (Greco et al., 2019) might be, along with the elastocaloric effect, the most promising alternative to vapor compression systems (Goetzler et al., 2014), due to the high adiabatic temperature change. Carvalho et al. (2018), for example, reported a 12 K temperature drop in the polydimethylsiloxane rubber (PDMS) when suddenly decompressed from 173 MPa to 0 MPa around room temperature. However, there is a lack of information and models in the literature to evaluate the applicability of these materials as solid-state refrigerants, which may justify why there were no prototypes of barocaloric refrigerators and heat pumps in operation when Greco et al. (2019) published their review on caloric cooling processes.

The recent work of Aprea et al. (2020) compared, via numerical simulations, the heating capacity of different i-caloric materials in an active caloric regenerator (ACR) with parallel plates geometry. The results also showed good perspectives for the mechanocaloric systems. Yet, it is worth noting here that this study was limited to a single regenerator geometry and that it neglected an important particularity of the elastomeric barocalorics: when applying the pressure on the elastomer, it has to be confined between rigid walls in order to restrain its deformation in the directions transverse to the pressure application. Under these conditions, high adiabatic temperature changes can be verified. Therefore, the ACR composed of polymeric elastomers must have solid (metallic) walls confining the elastomer, which will act as a thermal resistance between the barocaloric material and the working fluid.

The present paper aims to make up for this scarcity of theoretical models and numerical data concerning the thermodynamic performance of barocaloric elastomers when employed in cooling applications. A bidimensional and transient mathematical model to simulate the fluid flow and heat transfer, firstly developed to investigate parallel-plates active magnetic regenerators proposed by Oliveira et al. (2012), is modified and expanded to simulate an active barocaloric regenerator (ABR) with the same geometry and using an elastomer as the solid refrigerant. The influence of

some geometric parameters and operational conditions, such as mass flow rate and temperature span, on the cooling capacity is investigated and performance curves (cooling capacity as a function of the temperature span) are presented.

2. THE BAROCALORIC REFRIGERATOR

At this point, it is important to introduce some definitions. First, the name caloric materials, which is attributed to materials that experience a change in the level of disorder of some of their internal structures (e.g., magnetic sublattice or crystalline lattice) when subjected to a change of intensity of an applied field. The magnetocaloric materials are driven by a magnetic field. The electrocalorics are driven by an electric field. The mechanocalorics, in turn, work under a mechanical stress field variation. In the latter case, if this field is one of uniaxial tension, they are called elastocalorics. If it is one of hydrostatic pressure, they are barocaloric materials (BC) – (Takeuchi and Sandeman, 2015).

In most of the known caloric materials, the elevation of the field intensity results in the reduction of the correspondent internal disorder, which is equivalent to an entropy decrease if the process is isothermal. On the other hand, if the field is applied quickly (adiabatically), with zero entropy generation, the 2nd Law of Thermodynamics tells us that the process is isentropic, and therefore the temperature rises. To be applied in refrigerators, the caloric effect must be reversible, that is, the removal of the external field results in the cold down of the material. Two common metrics to measure the caloric effect of a material are then the isothermal entropy change (ΔS_T) and the adiabatic temperature variation (ΔT_{ad}) (Pecharsky and Gschneidner, 1999).

To illustrate how the BCE can be applied in cooling applications, consider a device having a hot heat exchanger (HHEX – at a fixed temperature T_H) and a cold heat exchanger (CHEX – at constant temperature T_C). In between, it is placed an active barocaloric regenerator composed of the elastomer processed in a given geometry, and of the working fluid responsible to exchange heat with the regenerator matrix and the thermal reservoirs. Thus, when synchronizing the compression/decompression cycle with the alternating fluid flow system, it is possible to establish a thermodynamic cycle. A scheme of this type of equipment operating in accordance with the Brayton cycle is shown in Figure 1, although other thermodynamic cycles can be employed (Trevizoli et al., 2016).

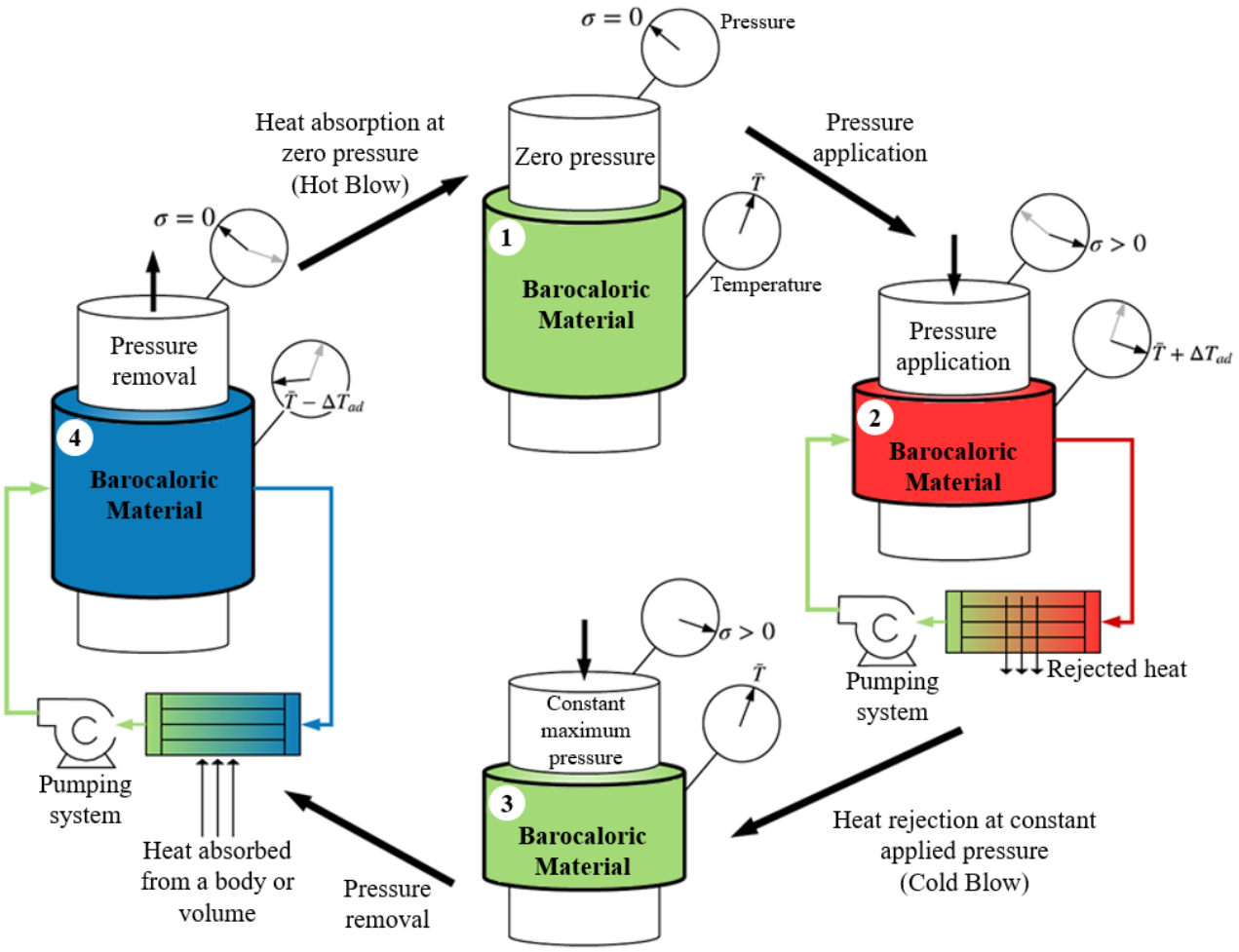

Figure 1. Schematic diagram of an active barocaloric regenerator (ABR).

In stage 1 (in Figure 1), there is no pressure on the material and its temperature is moderate (between the temperatures of the heat exchangers). The matrix is then compressed adiabatically reaching stage 2, of high hydrostatic pressure and temperature due to the BCE. Keeping the pressure constant, the fluid is then pumped from the CHEX to the HHEX (Cold Blow), absorbing heat from the regenerator, and rejecting it at the HHEX. At the end of this process, the regenerator bed will be at stage 3, of high compression stress and temperature again moderate. Removing the pressure adiabatically, the matrix reaches its minimum temperature due to the reversible (negative) caloric effect (stage 4). Now, kept at ambient pressure, the fluid is pumped from the HHEX to the CHEX (Hot Blow). In this process, the matrix returns to its initial condition while it absorbs energy from the heat transfer fluid, which in turn, gets to the CHEX colder than T_C, and thus, absorbing heat from a cold reservoir.

3. MATHEMATICAL MODEL

A mathematical model is proposed to study the fluid flow, the heat transfer and the thermodynamic performance of an ABR using as solid refrigerant the barocaloric elastomer PDMS (polydimethylsiloxane) rubber. The present model is an expansion of a previous work by Oliveira et al. (2012), developed to simulate active magnetic regenerators. Therefore, parallel plates geometry is considered as presented in Figure 2.

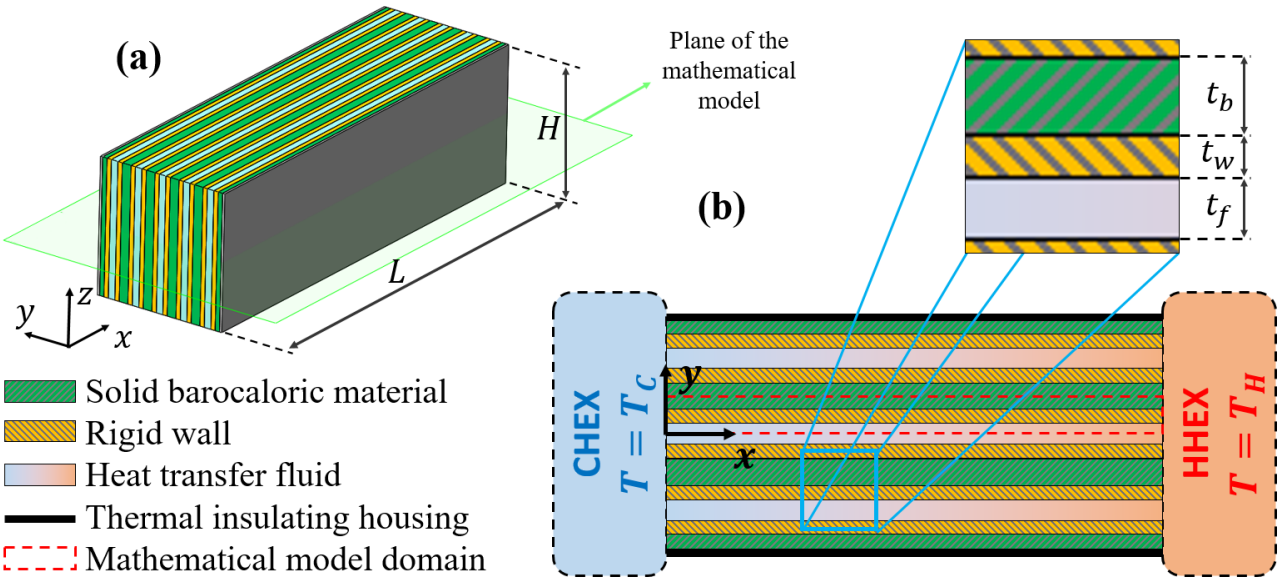

Figure 2. (a) Parallel plates regenerator; (b) Cross-section on the xy plane.

The compression of the BC material is done in the z direction, so there must be rigid walls of some thermal conductor material confining the elastomer to restrain its expansion in the y direction and establish a stress state close to the hydrostatic. The fluid (a mixture of water and additives) flows alternately between the walls in the x direction driven by a sinusoidal pressure gradient (oscillating flow). The height H of the matrix is considerably bigger than the thickness t_f of the flow channel and, added to this, regenerators are typically well thermally insulated from the external environment, thus the gradient of any physical quantity in the z direction is neglected, reducing the problem to a two-dimensional model in the xy plane, shown in Figure 2(b).

In order to simplify the problem even further, only one unit cell is modeled and simulated, i.e., the smallest geometry that repeats itself in the device, and the total results of extensive quantities can be obtained by multiplying the results of one unit cell by the number of cells in the matrix ($2N$). This unit cell is highlighted by red dashed lines in Figure 2(b), and includes all the length L of the duct, half elastomer plate (width of $t_b/2$), an entire rigid wall (width of t_w) and half flow channel ($t_f/2$). This reduction of the domain is equivalent to analyzing a regenerator with the end barocaloric plates having a thickness of $t_b/2$ and being perfectly insulated from the surroundings.

3.1 Fluid flow model

In addition to those already mentioned, other simplifications are adopted in order to model the oscillating flow: decoupling of the hydrodynamic model from the thermal problem, constant fluid properties, negligible body forces, laminar, one-dimensional and fully-developed flow. Furthermore, the governing equation is used in dimensionless form, resulting in the simplified Navier-Stokes equation (Eq. (1)) with the respective boundary (Eq. (2) and Eq. (3)) and initial (Eq. (4)) conditions (Oliveira et al., 2012).

$$\frac{1}{\phi}\frac{\partial u^*(y^*,\tau)}{\partial \tau} = 2\,cos(2\pi\tau) + \frac{\partial^2 u^*(y^*,\tau)}{\partial y^{*2}} \quad , \tag{1}$$

$$u^*(1,\tau) = 0 \quad , \tag{2}$$

$$\left.\frac{\partial u^*}{\partial y^*}\right|_{y^*=0} = 0 \quad , \tag{3}$$

$$u^*(y^*,0) = 0 \quad . \tag{4}$$

In equations (1) to (4), u^*, y^* and τ are the dimensionless forms of the fluid velocity in the x direction (u), the y coordinate and time (t), being defined, respectively, by equations (5), (6) and (7).

$$u^*(y^*,\tau) = \frac{u(y,t)}{(A_0 t_f^2)/(8\nu)} = \frac{u(y,t)}{3U/2} \quad , \tag{5}$$

$$y^* = y/(t_f/2) \quad . \tag{6}$$

$$\tau = t/P \quad , \tag{7}$$

In Eq. (5), ν is the kinematic viscosity and A_0 is the amplitude of the harmonic driving pressure gradient divided by the fluid density (ρ_f), that is: $-dP/dx = \rho_f A_0\, cos(2\pi\tau)$. $3U/2$ is the maximum fluid velocity that would be observed if the pressure gradient were kept constant and equal to its amplitude all the time, as in a steady-state Hagen-Poiseuille flow. P is the period of the sinusoidal cycle. The parameter ϕ is defined in Eq. (8), where $Re_{\omega(D_H)}$ is the kinetic Reynolds number, based on the hydraulic diameter ($D_H = 2t_f$) and $\omega = 2\pi/P$ is the angular frequency.

$$\phi = \frac{32\pi}{Re_{\omega(D_H)}} = \frac{32\pi}{\frac{D_H^2\omega}{\nu}} = \frac{32\pi}{\frac{(2t_f)^2\omega}{\nu}} \quad . \tag{8}$$

3.2 Heat transfer model

The thermal problem is modeled by the energy conservation equation simplified as follows. The thermophysical properties of both fluid and solid are constant. Regarding the fluid, viscous dissipation and longitudinal (x direction) heat conduction are neglected, once it can be shown through a scale-analysis, in accordance with the method of Costa (2002), that these effects are not important if compared to the advective energy transport and transverse (y direction) heat diffusion. Heat generation terms are also not present. Equations (9), (10) and (11) present the obtained energy equation in dimensionless form, written respectively for the fluid (subscript f), for the wall (subscript w) and for the barocaloric material (subscript b).

$$\frac{1}{Fo_{D_H,f}}\frac{\partial \theta_f}{\partial \tau} + \gamma Pe_{D_H}\frac{\partial \theta_f}{\partial x^*} = 16\frac{\partial^2 \theta_f}{\partial y^{*2}} \quad , \tag{9}$$

$$\frac{1}{Fo_{D_H,w}}\frac{\partial \theta_w}{\partial \tau} = \gamma^2\frac{\partial^2 \theta_w}{\partial x^{*2}} + 16\frac{\partial^2 \theta_w}{\partial y^{*2}} \quad , \tag{10}$$

$$\frac{1}{Fo_{D_H,b}}\frac{\partial \theta_b}{\partial \tau} = \gamma^2\frac{\partial^2 \theta_b}{\partial x^{*2}} + 16\frac{\partial^2 \theta_b}{\partial y^{*2}} \quad . \tag{11}$$

In the three previous equations, $Fo_{D_H,i} = \alpha_i P/D_H^2$ is the Fourier number, which depends on the thermal diffusivity $\alpha_i = k_i/\rho_i c_{p,i}$ of each corresponding material. $\gamma = D_H/L$ is a geometric parameter, $Pe_{D_H} = u(y,t)D_H/\alpha_f$ is the Péclet number, x^* is the dimensionless axial coordinate (Eq. (12)) and θ is the dependent variable – the temperature T normalized with the heat exchangers temperatures – defined by Eq. (13).

$$x^* = x/\mathrm{L} \quad , \tag{12}$$

$$\theta = \frac{T - T_C}{T_H - T_C} \quad . \tag{13}$$

It is considered that the fluid always enters the channel with the temperature of its heat exchanger of origin – Eq. (14).

$$\begin{cases} \theta_f(0, y^*, \tau) = 0 & u(y^*, \tau) \geq 0 \\ \theta_f(1, y^*, \tau) = 1 & u(y^*, \tau) < 0 \end{cases} . \tag{14}$$

At the upper $(+y)$ and lower $(-y)$ boundaries of the domain, and at the left $(-x)$ and right $(+x)$ boundaries of the solids conditions of symmetry/thermal insulation are applied – Eq. (15).

$$\left.\frac{\partial \theta_f}{\partial y^*}\right|_{y^*=0} = \left.\frac{\partial \theta_b}{\partial y^*}\right|_{y^*=1+\frac{t_w+t_b/2}{t_f/2}} = \left.\frac{\partial \theta_w}{\partial x^*}\right|_{x^*=0} = \left.\frac{\partial \theta_w}{\partial x^*}\right|_{x^*=1} = \left.\frac{\partial \theta_b}{\partial x^*}\right|_{x^*=0} = \left.\frac{\partial \theta_b}{\partial x^*}\right|_{x^*=1} = 0 \quad . \tag{15}$$

On the interfaces between different materials, there are conditions of heat flux and temperature continuity, represented by equations (16) to (19).

$$\theta_f|_{y^*=1} = \theta_w|_{y^*=1} \quad , \tag{16}$$

$$k_f \left.\frac{\partial \theta_f}{\partial y^*}\right|_{y^*=1} = k_w \left.\frac{\partial \theta_w}{\partial y^*}\right|_{y^*=1} \quad , \tag{17}$$

$$\theta_w|_{y^*=1+\frac{t_w}{t_f/2}} = \theta_b|_{y^*=1+\frac{t_w}{t_f/2}} \quad , \tag{18}$$

$$k_w \left.\frac{\partial \theta_w}{\partial y^*}\right|_{y^*=1+\frac{t_w}{t_f/2}} = k_b \left.\frac{\partial \theta_b}{\partial y^*}\right|_{y^*=1+\frac{t_w}{t_f/2}} \quad . \tag{19}$$

The discrete approach (Nielsen et al., 2011) is used for the implementation of the barocaloric effect, i.e., a step-like temperature variation is imposed on the BC material at the instants the pressure gradient inverts its signal, which according to Eq. (1), happen when $\tau = n + 0{,}25$ (pressure removal) and $\tau = n + 0{,}75$ (pressure application), with $n = 0{,}1{,}2{,}3$ ... being the number of the cycles. The amplitude of this step is a function of the variation of the compression stress $(\Delta\sigma)$ and of the temperature (T_b) immediately before the pressure change. The experimental data of $\Delta T_{ad}(T_b, \Delta\sigma)$ for the PDMS rubber presented by Carvalho et al. (2018) is used.

4. SOLUTION OF THE MATHEMATICAL MODEL

4.1 Analytical solution of the fluid flow model

The analytical solution of equations (1) to (4), obtained by Laplace Transform, was also given in Oliveira et al. (2012). For completeness of this text, the solution is equally shown here in Eq. (20),

$$u^*(y^*, \tau) = \frac{8\phi}{\pi} \sum_{i=1}^{\infty} \frac{(-1)^i}{2i-1} cos\left[\frac{(2i-1)\pi y^*}{2}\right] \times \int_{\tau}^{0} exp\left[-\frac{(2i-1)^2\pi^2\phi(\tau-\zeta)}{4}\right] cos(2\pi\zeta) d\zeta \quad , \tag{20}$$

where ζ is a dummy variable that disappears when the integral in the right-hand side is solved. The use of this solution allows the complete model to be solved faster (with less computational time) than if the flow field were calculated by a numerical method.

For the low kinetic Reynolds number used in this work, Eq. (20) results in a flow oscillation in phase with the pressure gradient, justifying the application of the barocaloric effect in the same instants that $cos(2\pi\tau)$ changes its signal. In this way, the cold blow takes place during the interval $n - 0{,}25 < \tau < n + 0{,}25$ and the hot blow in $n + 0{,}25 < \tau < n + 0{,}75$.

4.2 Numerical solution of the heat transfer model

As the model defined by equations (9) to (11) and (14) to (19) has no analytical solution, it is solved numerically with the well known Finite Volume Method (FVM) (Maliska, 1995), implemented in a code written in the Python 3 – Spyder programming language. The solution starts from the fluid velocities calculated beforehand with Eq. (20) for each finite volume. It's worth noting here that, as a structured mesh (rectangular elements) is used and the flow is treated as fully developed, only one fluid velocity per time step has to be calculated for all the volumes in a same row (same y^* position). Moreover, this velocity can be calculated only in the time steps of one cycle and then used repeatedly.

For the temporal discretization, the fully implicit formulation was applied. Correspondingly, the fluid velocities in the discretized equations are evaluated in the same instant that the θ's are being calculated in a given time step. The interpolation functions used to calculate the fluxes at the interfaces of the control volumes are the central differences scheme (CDS) for the diffusive terms and the upwind differencing scheme (UDS) for the advective terms.

This leads to one discretized equation for each finite volume in the form $A_P\theta_P = A_E\theta_E + A_W\theta_W + A_N\theta_N + A_S\theta_S + B$, resulting in a linear system, solved with the TDMA (TriDiagonal Matrix Algorithm). As recommended by Maliska (1995), it is considered that a time step has converged when Eq. (21), based on the residuals of the discretized equations, is satisfied. In this equation, j is the iterative level in the current time step and the subscripts nb and NB mean "neighbor", referring to the volumes E, W, N e S next to the volume P corresponding to each of the discretized equations. The convergence criteria ε in this work is fixed in $1\text{x}10^{-6}$.

$$\mathcal{R}^{j+1} = \sqrt{\sum \left(B + \sum A_{nb}\theta_{NB}^{j+1} - A_P\theta_P^{j+1}\right)^2} \leq \varepsilon \quad . \tag{21}$$

At the end of each hot blow ($\tau = n + 0{,}75$) the code checks two conditions: (i) if all nodal points in all time steps of the last cycle had a variation of T smaller than $5\text{x}10^{-3}$ K in relation to the previous cycle; (ii) and if the average cooling and heating capacities varied less than 0.5 % also comparing with the cycle before. If both conditions are satisfied, it is considered that the periodically developed regime is established and the simulation stops.

The average cooling capacity ($\bar{\dot{Q}}_C$) is the main metric of interest and is defined by Eq. (22), in which the term between brackets is the instantaneous cooling capacity ($\dot{Q}_C$) and N is the number of channels in the device. The min function assures that the integral is incremented only when heat transfer fluid gets to the cold reservoir, and not when fluid leaves the CHEX to enter the duct. The minus sign makes $\dot{Q}_C$ positive when refrigeration occurs. The average heating capacity ($\bar{\dot{Q}}_H$) is equated and implemented in the code in a similar manner.

$$\bar{\dot{Q}}_C = \frac{1}{P}\int_{(n-0{,}25)P}^{(n+0{,}75)P}\left[2.N\int_0^{t_f/2} -min(u(y,t),0)\rho_f c_f\left(T_C - T_f(0,y,t)\right)Hdy\right]dt \quad . \tag{22}$$

4.3 Mesh refinement study

To perform the mesh independence analysis, the operating parameters presented in Table 1 were used.

Table 1. Operational parameters for the mesh independence study.

T_H, K	T_C, K	$\Delta\sigma$, MPa	$\bar{\dot{m}}$, kg/h	P, s
300,65	295,65	173	32.1	10

The mass flow rate $\bar{\dot{m}}$ is defined in Eq. (23),

$$\bar{\dot{m}} = \frac{1}{P/2}\int_{(n-0{,}25)P}^{(n+0{,}25)P}\left[2.N\int_0^{t_f/2} u(y,t)\rho_f\, Hdy\right]dt \quad . \tag{23}$$

In Table 2, the thermophysical properties of the materials, and the proposed geometric parameters used in this work are presented.

Table 2. Thermophysical properties and the proposed geometric parameters of the ABR simulated in this work.

	Heat transfer fluid (Water)	**Metallic wall (Aluminum 7075-T62)**	**Barocaloric material (PDMS rubber)**
k**, W/m/K**	0.5948	130	0.1511
ρ**, kg/m^3**	997.1	2810	1028
c_p**, kJ/kg/K**	4183	960	1532
μ**, kg/m/s**	8,905.10^{-4}	-	-
Reference	Software EES (Engineering Equation Solver)	ASM International (1990)	Carvalho et al. (2018) and Mark (1999)
Thickness, mm	0.125	1.0	1.0
L**, mm**	200		
H**, mm**	10		
N	20		

Table 3 shows the dependence of $\bar{Q}_C$, $\bar{Q}_H$ and the computation time (t_{comp}) with the spatial mesh. Simulations were performed using a computer configuration with a processor Intel Core i5-5200U CPU @ 2,20 GHz and a 64 bits operational system. n_t is the number of time steps in each cycle. n_x and n_y are the numbers of control volumes in the x^* and y^* directions. The mesh is homogeneous in the longitudinal (x^*) direction. In the y^* direction, in turn, one-fourth of the volumes are placed in the fluid phase and the remaining ones are distributed as homogeneously as possible to the two solids.

Table 3. Influence of the spatial mesh on the simulation results.

Mesh	n_x	n_y	n_t	$\bar{Q}_C$**, W**	$\Delta\bar{Q}_C$**, %**	$\bar{Q}_H$**, W**	$\Delta\bar{Q}_H$**, %**	t_{comp}
1	80	24	100	15.19	-	24.45	-	4.30 min
2	160	48	100	15.90	+4.29	25.29	+3.42	44.75 min
3	240	72	100	16.12	+1.38	25.56	+1.07	3.33 hrs
4	320	96	100	16.22	+0.62	25.69	+0.54	10.11 hrs

As a conclusion from Table 3, Mesh 3 is selected because a more refined mesh (Mesh 4) presented little improvements on the target results while increasing in about three times the simulation time. In this work, the qualitative tendencies and the physical behavior of the ABR are of more interest than extremely precise values of the cooling and heating capacities.

The results of the temporal mesh refinement study are then registered in Table 4. The same reasoning that motivated the choice of Mesh 3 in the spatial refinement, justify the selection of Mesh 7 in the temporal refinement. Thus the results in the following section were all calculated with this domain discretization: $n_x = 240$, $n_y = 72$ and $n_t = 800$.

Table 4. Influence of the temporal refinement on the simulation results.

Mesh	n_x	n_y	n_t	$\bar{Q}_C$**, W**	$\Delta\bar{Q}_C$**, %**	$\bar{Q}_H$**, W**	$\Delta\bar{Q}_H$**, %**	t_{comp}
3	240	72	100	16.12	-	25.56	-	3.33 hrs
5	240	72	200	17.33	+7.53	26.63	+4.19	3.62 hrs
6	240	72	400	18.03	+4.00	27.09	+1.73	3.89 hrs
7	240	72	800	18.33	+1.69	27.26	+0.66	5.47 hrs
8	240	72	1600	18.50	+0.94	27.19	-0.26	7.60 hrs

5. RESULTS

The results presented in this section stand for the evaluation of the cycle cooling capacity as a function of different geometric (PDMS and wall thicknesses) or operating parameters (mass flow rate and temperature span, $\Delta T = T_H - T_C$). The results presented in Table 5 analyzed first the dependence of $\bar{Q}_C$ in respect to the PDMS thickness (keeping all the remaining parameters fixed, which values are in tables 1 and 2); and second, the evaluation of $\bar{Q}_C$ as the wall thickness varies (all the remaining parameters are fixed - see tables 1 and 2). Table 5 also presents the percentual variations relative to the reference geometry (bold) of Table 2.

Looking at the cooling capacity dependence in respect to the PDMS thickness (first three columns in Table 5), one can note that there is a peak value at $t_b = 1$ mm. If this thickness is too small (small thermal capacity, e.g., 0.5 and 0.25 mm) the elastomer warms up too fast during the hot blow, tending to thermal equilibrium with the fluid stream, which impacts negatively on the regenerative refrigeration cycle (same analysis can be conducted to the cold blow). On the other

hand, if t_b gets too large (e.g., 2 mm), a large temperature gradient is verified along the elastomer thickness, due to its low thermal conductivity. For example, at the center of the PDMS (symmetry plane) the temperature may still be high at the end of the cold blow. This behavior is consistent with the large Biot number found in some configurations of the PDMS plate. As a direct consequence, when the pressure is removed and the BC material cools down (due to the negative barocaloric effect), the core part will not achieve the designed low temperatures, which are actually considerably higher than the geometry with $t_b = 1$ mm. Thus, the refrigerant effect is lower, as well as the cooling capacity. The same analysis can be performed considering the remaining part of the cycle (hot blow and pressure application).

Table 5. Influence of selected parameters on the cooling capacity.

t_b, mm	$\dot{\bar{Q}}_C$, W	$\Delta\dot{\bar{Q}}_C$, %	t_w, mm	$\dot{\bar{Q}}_C$, W	$\Delta\dot{\bar{Q}}_C$, %
2	6.65	-63.7	3	0.21	-98.8
1	**18.33**	-	2	6.94	-62.1
0.5	11.46	-37.5	**1**	**18.33**	-
0.25	-1.79	-109.8	0.5	24.04	+31.1

From the results for the wall thickness variation (last three columns of Table 5), it is clear that as t_w tends to zero, the cooling capacity increases considerably. As the wall gets thicker, two important effects over the thermal performance of the system are verified: i) the increasing of the conduction thermal resistance; ii) the increasing of the thermal mass of the solid wall. The latter was identified as the main effect. A large thermal mass represents a large thermal inertia. For example, after the pressure removal, the PDMS gets cooler due to the negative barocaloric effect, while the wall is at a higher temperature. Thus, the refrigerant effect must be used in a first moment to cool down the solid wall, and after some time, starts to remove heat from the hot fluid stream. As a result: a) a good portion of the refrigerant effect is "consumed" by the solid wall; b) long cycle periods are necessary to effectively cool down the fluid stream that enters the cold reservoir. In some cases, the thermal mass of the wall gets so large that no cooling capacity is observed (negative values).

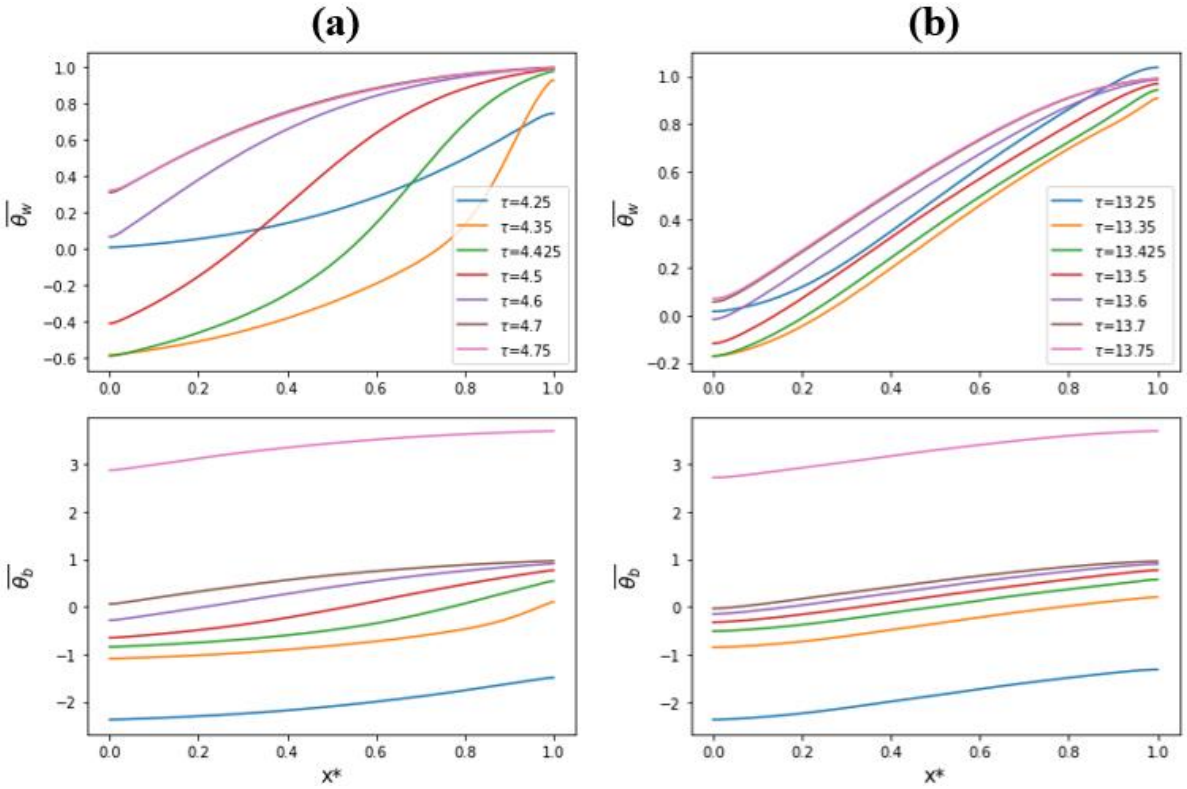

Figure 3. Elastomer and wall average temperatures during the hot blow: (a) $t_w = 0.5$ mm; (b) $t_b = 2$ mm.

To illustrate this effect, Figure 3 shows the dimensionless average temperature profiles along the x^* direction considering $t_w = 0.5$ mm in Figure 3(a) and $t_w = 2$ mm in Figure 3(b). Here, only part of the cycle is evaluated (from the instant immediately after the decompression until right after the next compression). $\bar{\theta}_w$ and $\bar{\theta}_b$ are the average temperatures of the solids taken in the y^* direction. In both cases, $\bar{\theta}_b$ increases approximately the same amount from $\tau = n + 0.25$ (when the cooling BCE occurs) to $\tau = n + 0.35$, i.e., the same amount of energy was absorbed. However, due

to the lower thermal inertia of the thinner wall, it cooled down a lot more (Figure 3a) than the thicker wall (Figure 3b) in the same time interval, becoming more prone to remove heat from the water.

Figure 4(a) presents the so-called performance curves, which evaluate $\bar{Q}_C$ as a function of the temperature span ($\Delta T = T_H - T_C$). Several performance curves are shown for different mass flow rates, ranging from 16 to 80 kg/h. ΔT was varied by changing the CHEX temperature at 5 K increments, while T_H was fixed at 300.65 K. All the remaining conditions, as in tables 1 and 2, are fixed.

The performance curves in Figure 4(a) are quite similar to those observed for active magnetic regenerators (AMRs) published elsewhere for parallel plates geometry (Oliveira et al., 2012): the $\bar{Q}_C$ dependence with ΔT has a linear trend, where at $\Delta T = 0$, a maximum cooling capacity is obtained ($\bar{Q}_{C,max}$); while at $\bar{Q}_C = 0$ (no-load conditions) a maximum temperature span (ΔT_{max}) is found. These results are then reorganized in Figure 4(b), which presents $\bar{Q}_{C,max}$ and ΔT_{max} as functions of the mass flow rate. Notice that, ΔT_{max} values were calculated by linear interpolation/extrapolation while $\bar{Q}_{C,max}$ resulted directly from the simulations. Again, the results in Figure 4(b) are similar to those found for parallel plates AMRs.

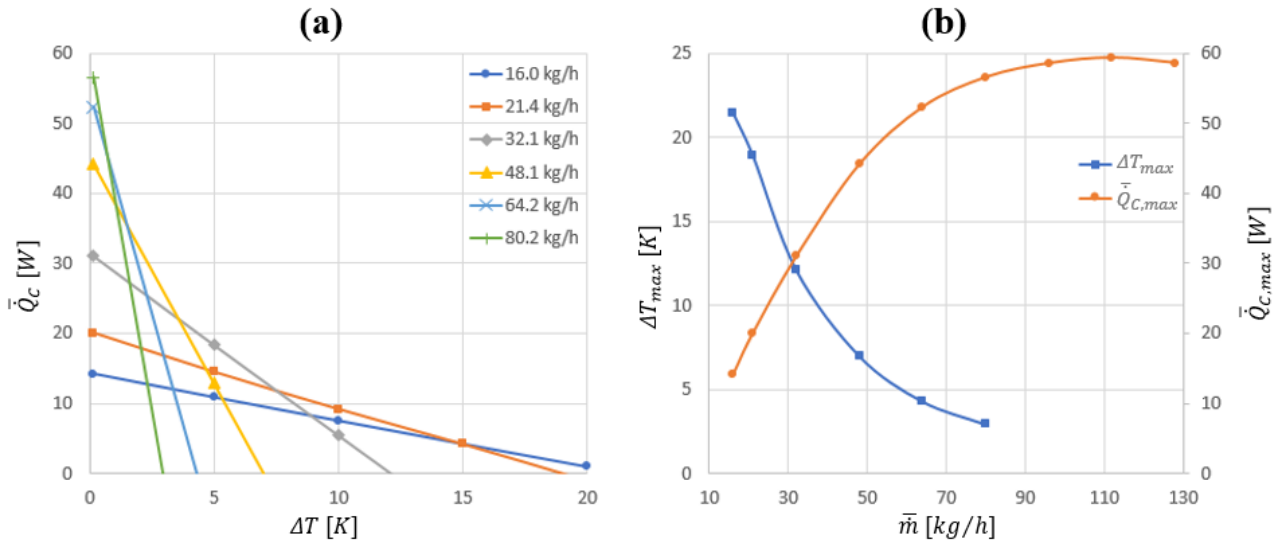

Figure 4. (a) Average cooling capacity as a function of ΔT; (b) Maximum temperature span and maximum average cooling capacity as functions of average mass flow rate.

Although general results presented for the in-study ABR are similar to AMRs with the same geometry, the performance curves for the ABR are away from the expected initially. One of the main limitations of magnetic refrigeration is the low magnetocaloric effect intensity (around 3 K/T), which is only observed around the Curie temperature. For temperatures apart from the Curie point, the magnetocaloric effect is even lower. The barocaloric effect, in turn, measured for PDMS at 173 MPa pressure variation is around 13 K at temperatures ranging from 240 K to 340 K.

However, experimental results for parallel plates AMRs using gadolinium, already presented maximum temperature span of around 20 K, when the peak ΔT_{ad} was about 4.0 K for a field variation of 1.5 T (Trevizoli et al., 2017). In this case, thermal regeneration was quite successful, increasing by 5 times the ΔT_{ad} of gadolinium. The in-study ABR, on the other hand, considering the proposed conditions and numerical simulations, presented a maximum 21 K span, but the peak ΔT_{ad} is 13 K. This result indicates that thermal regeneration is less effective in the present ABR, pointing that other barocaloric materials with better properties (read thermal conductivity and ΔT_{ad}), as well as novel ABR geometries or concepts, are necessary to overcome the thermal barriers discussed in this work. In addition to that, the simulations considered thin wall thickness ($\leq$ 3 mm), which is not suitable in a real prototype able to support pressure levels of 173 MPa. Thicker walls are necessary; however, the prototype would not be able to present useful cooling capacities.

6. CONCLUSIONS

A two-dimensional transient model to simulate the conjugate fluid flow and heat transfer problems in an ABR was proposed in this paper. An analytical solution was used for the hydrodynamic mathematical model, which reduces the computation effort needed to perform the simulations. The heat transfer problem was dealt with using the FVM. After a fine enough mesh was selected, simulations were executed to analyze the influence of some input parameters on the device performance.

It was shown that, for a given set of fixed parameters, there must be an optimum barocaloric plate thickness that maximizes the cooling capacity. Additionally, in the cases presented here, the average cooling power raised monotonically with the metallic wall thickness reduction. These results, however, do not take into account design considerations. In a prototype, the choice for the wall thickness should also be based on structural analysis. Concerning the caloric material, operational problems could come up when compressing repeatedly a very thin layer at the high pressure needed. With a thicker elastomer plate, it could be difficult to achieve the force required to compress the material in a compact equipment. Nevertheless, prototype design was not the main objective of this analysis, but rather to show the importance of parameters that have not received due attention in other works.

The analysis of the refrigeration capacity as a function of the temperature span and the mass flow rate has predicted a maximum temperature amplitude of 21.4 K for the proposed theoretical ABR, indicating that the thermal regeneration may have low effectiveness in the proposed configuration, associated with the large thermal mass imposed by the solid wall. Nonetheless, barocaloric refrigeration is a new field of study, and novel prototypes concepts and new barocaloric materials must be evaluated towards the development of high-efficiency barocaloric refrigerators.

7. ACKNOWLEDGEMENTS

The authors would like to thank CAPES for the scholarship granted to Pedro H. O. Faria, also to thank ABCM for the scholarship granted to Kimi S. Portugal through the "*Programa ABCM de Bolsas de Iniciação Científica - PABIC*".

8. REFERENCES

Aprea, C. et al., 2019. The employment of caloric-effect materials for solid-state heat pumping. *International Journal of Refrigeration*, v. 109, p. 1-11.

ASM International, 1990. *ASM Handbook: properties and selection: nonferrous alloys and special-purpose materials*. 10. ed. [S.l.]. v.2.

Calm, J. M., 2008. "The next generation of refrigerants – historical review, considerations, and outlook". *International Journal of Refrigeration*, v. 31, n. 7, p. 1123–1133.

Carvalho, A. M. G. et al., 2018. "Giant room-temperature barocaloric effects in PDMS rubber at low pressures". *European Polymer Journal*, v. 99, p. 212-221.

Costa, V. A. F., 2002. "A time scale-based analysis of the laminar convective phenomena". *International Journal of Thermal Sciences*, v. 41, n. 12, p. 1131-1140.

Coulomb, D., 2006. *Refrigeration: The challenges associated with sustainable development – Proceedings of the 6th International Conference on Compressors and Coolants held in Casta Papiernicka, Slovak Republic, September 27-29, 2006*.

Goetzler, W. et al., 2014. "Alternatives to Vapor-Compression HVAC Technology". *ASHRAE Journal*, v. 56, n. 10, p. 12-23.

Greco, A. et al., 2019. "A review of the state of the art of solid-state caloric cooling processes at room-temperature before 2019". *International Journal of Refrigeration*, v. 106, p. 66-88.

International Institute of Refrigeration, 2019. *38th Note on Refrigeration Technologies: The Role of Refrigeration in the Global Economy*. Paris: IIF-IIR, 2019. Available at: <https://iifiir.org/en/fridoc/142028>. Accessed 09 Nov. 2020.

Maliska, C. R., 1995. *Computational heat transfer and fluid mechanics: fundamentals and generalized coordinates* (in Portuguese). [Florianópolis]: LTC.

Mark, J. E., 1999. *Polymer data handbook*. New York: Oxford University Press.

Nielsen, K. K. et al., 2011. "Review on numerical modeling of active magnetic regenerators for room temperature applications". *International Journal of Refrigeration*, v. 34, n. 3, p. 603–616.

Oliveira, P. A.; Trevizoli, P. V.; Barbosa Jr., J. R.; Prata, A. T., 2012. "A 2D hybrid model of the fluid flow and heat transfer in a reciprocating active magnetic regenerator". *International Journal of Refrigeration*, v. 35, n. 1, p. 98-114.

Pecharsky, V. K., Gschneidner, Jr. K. A., 1999. "Magnetocaloric effect and magnetic refrigeration". *Journal of Magnetism and Magnetic Materials*, 200, 44–56.

Takeuchi, I.; Sandeman, K., 2015. "Solid-state cooling with caloric materials". *Physics Today*, v. 68, n. 12, p. 48-54.

Trevizoli, P.V. et al., 2016. "Magnetic heat pumps: an overview of design principles and challenges". *Science and Technology for the Built Environment*, v. 22, n. 5, p. 507–519.

Trevizoli, P.V. et al., 2017. "Performance assessment of different porous matrix geometries for active magnetic regenerators". *Applied Energy*, v. 187, p. 847-861.

9. RESPONSIBILITY NOTICE

The authors are the only responsible for the printed material included in this paper.